95 N6

EFFECTS OF POWER CONVERTER PARASITIC COMPONENTS ON CONDUCTED EMI

G. Grandi, I. Montanari, U. Reggiani
DIPARTIMENTO DI INGEGNERIA ELETTRICA
Viale Risorgimento 2, 40136 - BOLOGNA (Italy)

Abstract: This paper deals with conducted Electromagnetic Interference (EMI) produced by power electronic converters. Both differential- and common-mode components of the conducted emissions are considered. In particular, the analysis is focused on converters controlled with PWM techniques and supplied by a DC source. A circuit model which takes account of parasitic components is proposed for a switching cell that is the basic structure of this kind of converters. The values of the parasitic parameters (inductances and capacitances) are obtained by measurements, field analysis or both. This model permits the influence of the different parasitic parameters to be investigated. The simulations carried out by PSpice are compared with the corresponding experimental data obtained from a DC chopper prototype. The good agreement between the numerical and experimental results proves that the proposed equivalent circuit allows the prediction of the main conducted EMI phenomena with sufficient accuracy.

1. Introduction

When studying EMC problems in static converters, particular attention has to be paid in the converter model. It must take account of the non-ideal behavior in the HF range of both the electronic devices and the passive elements of the circuit [1,2]. The presence of HF current and voltage components is mainly due to the high switching speed of static devices. In particular, high values of dv/dt cause HF current components in main and parasitic capacitances ($i_c = C \cdot dv/dt$), whereas high values of di/dt generate HF voltage components in main and parasitic inductances ($v_l = L \cdot di/dt$). These HF components meet unexpected propagation paths due to the presence of parasitic elements.
Some difficulties may arise when evaluating parasitic parameters such as stray inductances of connecting wires, parasitic inductances of DC smoothing capacitors, and coupling capacitances between each power switch and the ground. The values of these parameters can be obtained by measurements, field analysis or both.
The theoretical and numerical analysis carried out on realistic circuit models of power converters allows the prediction of the dynamic behavior including conducted EMI [3,4].
For an accurate design of the converter according to EMC standards and emission limits, it is necessary to determine the amplitude of voltage and current harmonics. If EMC requirements are not satisfied, actions are needed. In this case, it is possible to modify the layout of the converter, to introduce additional reactive components, and to design an appropriate input filter [1,2].
The aim of this paper is to present a detailed circuit model of a switching cell that is the basic structure of most power converters. This cell is depicted in Fig.1 and represents a typical DC chopper. The methods employed to obtain the correct value of every electric parameter are discussed. Utilizing the proposed model, it is possible to perform numerical simulations with PSpice.
The influence of each parasitic parameter on conducted EMI is emphasized. In particular, the conducted interferences on the DC bus are investigated. The basic switching cell is validated by comparing the calculated results with experimental data. In both simulations and experimental tests, two Line Impedance Stabilization Networks (LISNs) are employed in order to standardize results.

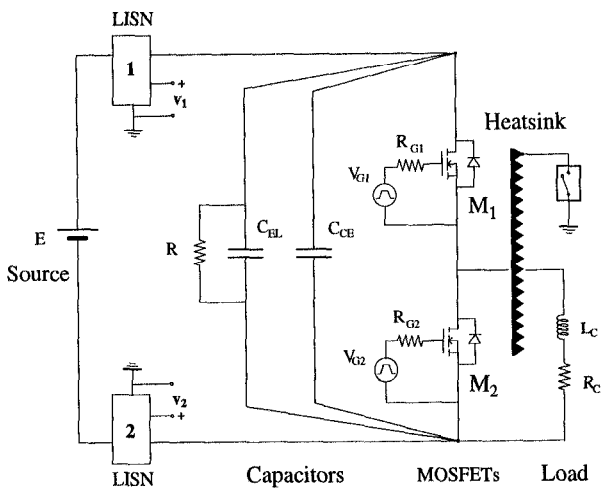

Fig.1: Basic structure of the switching cell

2. HF parasitic components

For an accurate EMC analysis of the converter, it is necessary to take HF parasitic components into account [5]. Fig.2 shows the HF equivalent circuit of the basic switching cell. The mean parasitic components of this circuit are

1. *Stray inductances of the connecting wires.* These parameters affect the total inductance of the circuit loops and strongly depend on the converter layout. It is possible to evaluate these inductances by the analytical formula for two parallel straight cylindrical conductors or for a circular or rectangular single-turn loop. Typical values for power switch leads are 5÷20 nH.

2. *Parasitic inductances of the capacitors.* It is not usually possible to evaluate these inductances analytically, but they

can be measured by means of impedance analyzers. Typical values are 5÷20 nH for ceramic capacitors and 30÷100 nH for large electrolytic capacitors. A parallel connection of both capacitor types is usually employed to obtain a large equivalent capacitance with a low equivalent parasitic inductance.

3. *Parasitic capacitances between the cell and the ground.* The ground potential may be introduced (for safety reasons) by the heatsink of the power switches and the metallic chassis. The values of these capacitances can be evaluated by means of the parallel-plate capacitor formula. They depend on the size and geometry of the power switches.

The converter analyzed in this paper contains one branch consisting of two power MOSFETs with intrinsic power diodes that provide for the free-wheeling path. The effects of the MOSFET (and diode) internal capacitance is included in PSpice models, whereas the values of the internal inductances are given by the data sheet and have to be introduced in the circuit model of the converter.
The PSpice built-in models for power switches have been chosen in order to simulate the switch characteristics that mainly affect EMI emissions

1. *Turn-on and turn-off transients.*
2. *Off-state output capacitance.*
3. *Diode reverse recovery.*

More accurate models can be found in literature (i.e. Power Diode [6], MOSFET and IGBT [7]), but the complexity of their equivalent circuits introduces difficulties and does not improve the EMC analysis substantially.
In literature the influence of some HF parasitic components on the so called *EMI energy* has been analyzed [8], but the correlation between the values of these parameters and the shape and amplitude of the harmonic spectrum has not been emphasized. As it will be clear in the following, variations in parasitic components may slightly affect the EMI energy but strongly modify the EMI spectrum. This is mainly due to changes in resonant frequencies among the main and parasitic reactive components (L and C) of the power converter.

3. Converter model and simulations

Fig.2 shows a chopper model including HF parasitic components. A switching cell with a similar configuration has been analyzed in [9].

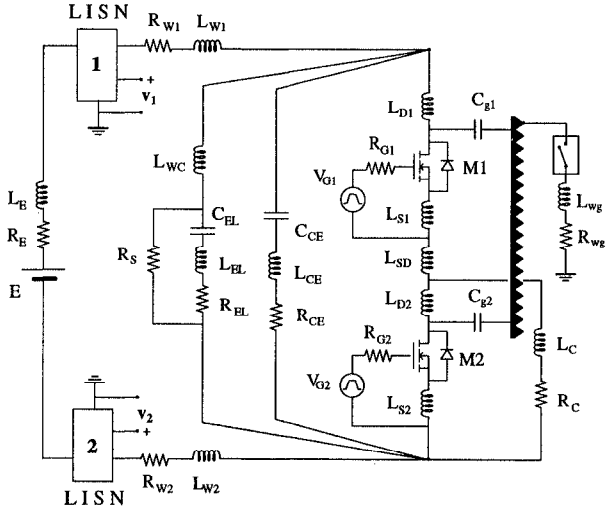

Fig.2: Chopper HF model with parasitic components

The topology of the adopted LISN (50/250 mH, 20A-500V) is depicted in Fig.3. The values of the main and parasitic parameters of both the chopper and the LISN used for the numerical analysis are given in Tab.I and Tab.II of the Appendix. The LISN is usually built taking care of minimizing HF parasitic effects. In this paper, the LISN components are considered as ideal elements.

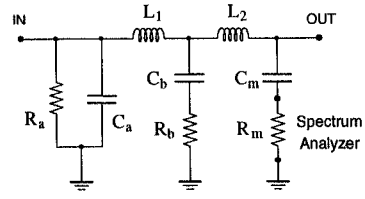

Fig.3: Scheme of the adopted LISN

The circuit simulator used for the computations was the Windows-version 6.2k of PSpice.
The behavior of the chopper has been investigated in the frequency range of 100 kHz - 40 MHz. The analysis has shown that the switching frequency and the duty-cycle do not affect the interference level in this range of frequency. Therefore, the reasonable values of 10 kHz for the switching frequency and of 60% for the duty-cycle have been assumed. The rise and fall times of the MOSFETs have been assumed to be equal to 100 ns and 200 ns, respectively.
In Fig.4 the loops responsible of the resonances that will be examined in the following analysis are highlighted.
In order to emphasize the influence of the different parasitic components of the realistic equivalent circuit of Fig.2, at first the heatsink has been supposed to be non-connected to ground. In this case, only differential-mode currents are present, being prevented any current path through the ground. Fig.5 shows the corresponding conducted emission spectrum. As it is possible to see, the spectrum emphasizes the presence of two peaks at the frequency of about 710 kHz and 31.8 MHz with an amplitude of 95 dBμV and 64 dBμV, respectively.
It has been found that the peak at lower frequency is due to the series-resonant loop (loop 1 in Fig.4) consisting of the ceramic and electrolytic capacitors, their internal parasitic components and the stray inductance of the connecting wires. Only the capacitance of the ceramic capacitor together with the overall stray inductance of the loop affects the resonant frequency. In fact, this capacitor is in series with an electrolytic capacitor having a capacitance of many orders of magnitude higher (e.g., 3300 μF vs. 0.33 μF).

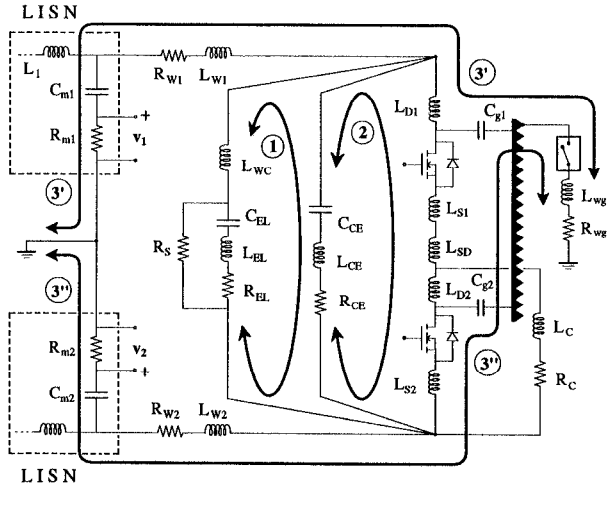

Fig.4: Chopper equivalent circuit with HF resonant loops

The peak at higher frequency is related to a series resonance in the loop (loop 2 in Fig.4) that consists of the power switches and the parallel connection of the two branches containing the electrolytic and ceramic capacitors. In any instant, one of the two switches is off and its model is reduced to an off-state capacitance. The other switch is on and is equivalent to a very low on-state resistance. The capacitances of both electrolytic and ceramic capacitors do not affect this resonant frequency, because the off-state capacitance of the switch has a much lower value and dominates the phenomenon (e.g., 0.8 nF vs. 0.33 μF). Furthermore, the electrolytic capacitor usually has an overall stray inductance (internal and external) much higher than that of the ceramic capacitor (e.g., 133 nH vs. 12 nH). Hence, the ceramic capacitor branch dominates this phenomenon and the resonant loop is composed of this branch and the power switches.

Connecting the heatsink to ground, the cell equivalent circuit changes and, consequently, a different conducted emission spectrum should be expected. In particular, also common-mode currents can flow now. The calculated emission spectrum is shown in Fig.6. It is possible to observe a further peak at the frequency of about 12.7 MHz with an amplitude of 80 dBμV. This resonance is introduced by the connection of the heatsink and the LISNs to ground. The corresponding resonant loop (common-mode loop) consists of the series connection of the ground wire with the parallel connection of two symmetrical branches of the equivalent circuit (branches 3' and 3'' in Fig.4). Each of these two branches contains the parasitic capacitance between a switch and the grounded heatsink, and the stray inductance of the connecting wire between the cell and a LISN. The ground wire is characterized by the parameters R_{wg} and L_{wg}.

In order to verify the previous analysis, the differential- and common-mode components of the total conducted emission have been calculated separately on the basis of the LISNs signals v_1 and v_2. The corresponding spectra are shown in Figs.7(a) and 7(b), respectively, and are related to the case of grounded heatsink. The spectrum of the differential-mode component shown in Fig.7(a) is practically equal to the spectrum of Fig.6 obtained when the heatsink is insulated. This proves that the differential-mode emission is practically not affected by the connection of the heatsink to ground. The spectrum of the common-mode component shown in Fig.7(b) highlights the resonant peak at 12.7 MHz discussed above.

In order to verify the effects of the parasitic components on conducted EMI, simulations with different values of the parasitic components have been performed. The results of these simulations, obtained with the heatsink connected to ground, are shown in the set of figures from Fig.8 to Fig.11.

For every case considered, both differential- and common-mode components of the conducted emissions are shown. Hence, the comparison has to be made with Fig.7.

Fig.8 concerns the case of a variation in the stray inductance of the electrolytic capacitor branch. In particular, the inductance L_{WC} of the connecting wires is reduced from 100 to 30 nH (for example, this change corresponds to a shorter connection between the capacitor and the switching branch). As shown in the figure, the stray inductance of the electrolytic capacitor branch practically affects only the differential-mode resonant peak at lower frequency. The peak amplitude decreases for decreasing values of the stray inductance, whereas the frequency of the peak increases according to the self-resonant frequency of the loop 1 shown in Fig.4.

Fig.9 is related to a change in the stray inductance of the switches branch. In particular, the inductance L_{SD} of the connecting wire between the switches is increased from 0 to 20 nH (for example, this change is obtained with a longer switch-to-switch connecting wire). As shown in this figure, the stray inductance of the switches branch practically affects only the differential-mode resonant peak at higher frequency. The peak amplitude increases for increasing values of the stray inductance, whereas the frequency of the peak decreases according to the self-resonant frequency of the loop 2 shown in Fig.4.

Fig.10 concerns the case of a variation in the stray inductance of the ceramic capacitor branch. In particular, the parasitic inductance L_{CE} is increased from 12 to 30 nH (for example, this increase occurs employing a worse quality capacitor). As shown in this figure, the parasitic inductance of the ceramic capacitor affects both peaks of the differential-mode component. In fact, this capacitor is involved in both loops 1 and 2 of Fig.4. The amplitude of the peak at higher frequency and the interference level in the central frequency range increase. The frequency of this peak decreases according to the self-resonant frequency of the loop 2 shown in Fig.4. The effects on the peak at lower frequency are smaller, because the parasitic inductance of the ceramic capacitor has a lower influence on the resonant loop 1 of Fig.4. In fact, the stray inductance of the electrolytic capacitor has a much higher value.

In Fig.11 the effects of a variation in the stray capacitances between the switches and the heatsink are considered. In particular, the stray capacitances C_{g1} and C_{g2} are decreased from 60 to 30 pF (for example, this reduction corresponds to a greater thickness of the insulation layer between the switches and the heatsink with a consequent worse thermal coupling). As shown in this figure, the stray capacitances practically do not affect the differential-mode component, whereas they influence the common-mode component. We observe a decrease in the overall interference level. Also the peak amplitude decreases, whereas the frequency of the peak increases. This agrees with the self-resonant frequency of the common-mode loop that consists of the series connection of the ground wire with the parallel connection of the branches 3' and 3'' shown in Fig.4.

A similar analysis can be developed for single- and three-phase inverters. In this case, two or three switching branches have to be taken into account. A more complex model is then obtained but the main results of the investigation concerning both differential- and common-mode components of the conducted EMI are still valid.

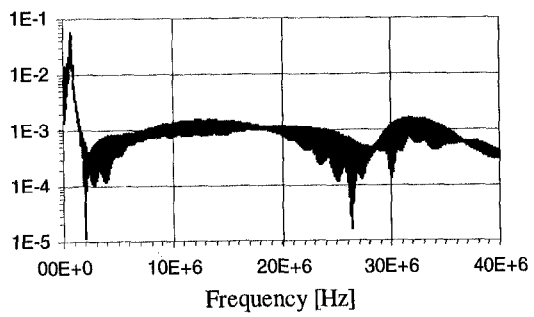

Fig.5: Calculated emission spectrum with heatsink non-connected to ground.

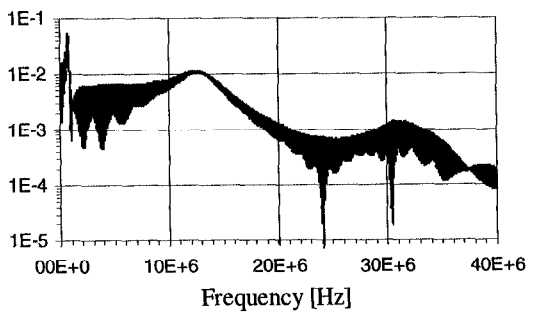

Fig.6: Calculated emission spectrum with heatsink connected to ground.

Calculated emission spectra with the heatsink connected to ground and for different values of the parasitic components

Differential-mode component **Common-mode component**

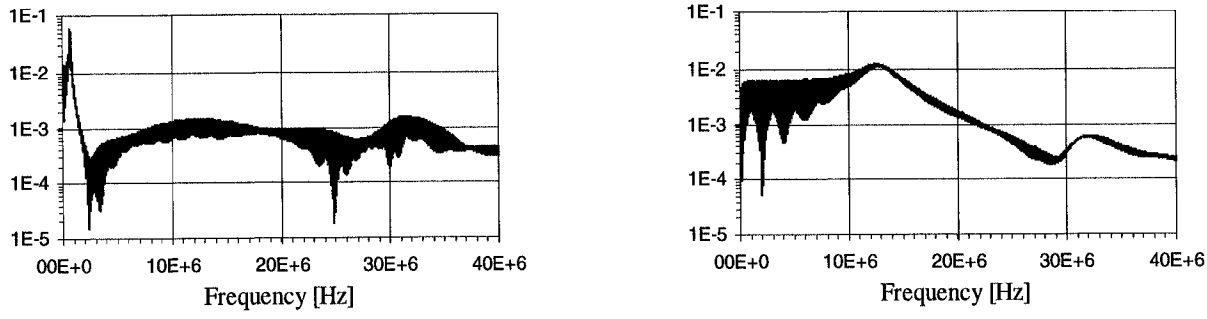

(a) **Fig.7: Basic values for the parasitic parameters** (b)

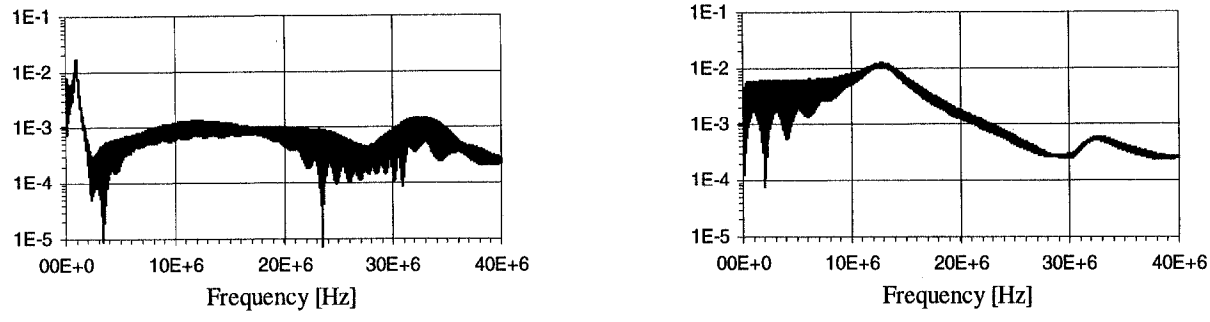

(a) **Fig.8: L_{WC} decreases from 100 to 30 nH** (b)

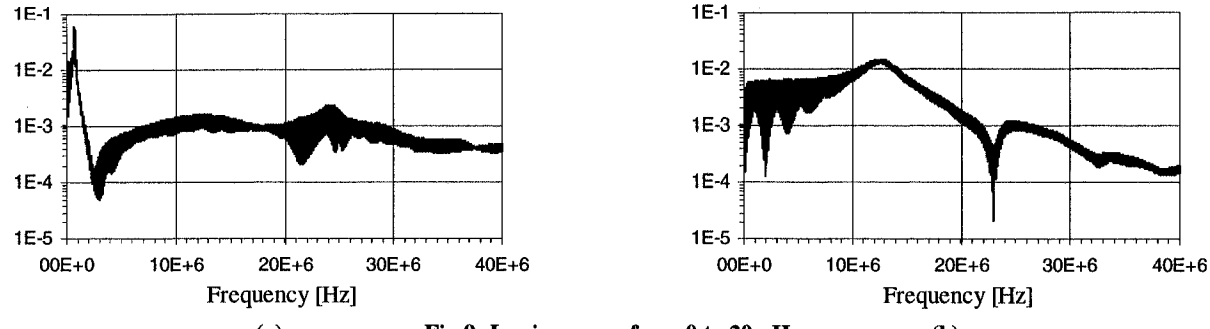

(a) **Fig.9: L_{SD} increases from 0 to 20 nH** (b)

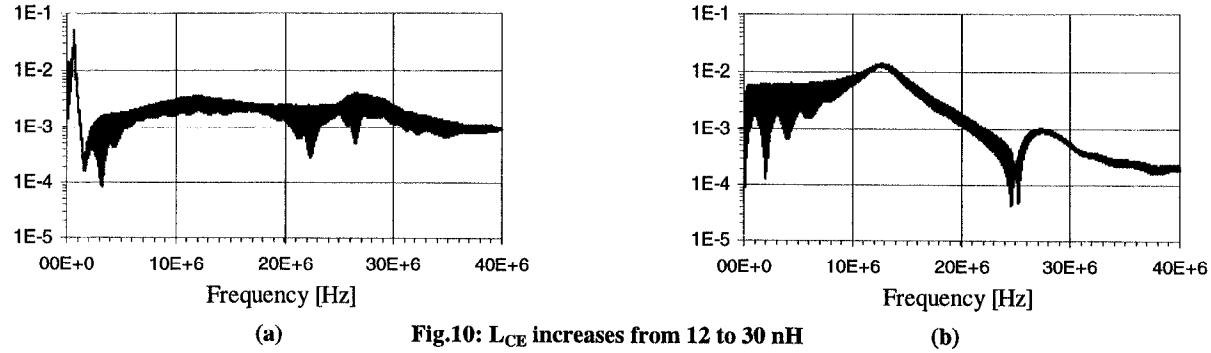

(a) **Fig.10: L_{CE} increases from 12 to 30 nH** (b)

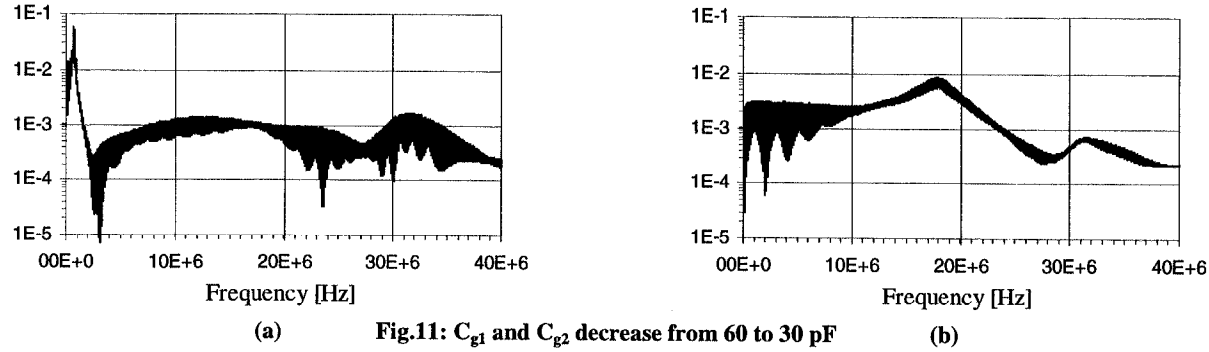

(a) **Fig.11: C_{g1} and C_{g2} decrease from 60 to 30 pF** (b)

4. Experimental results

In order to validate both the numerical results and the theoretical analysis, a DC chopper prototype was built on the basis of the circuit represented in Fig.1.

The experimental set-up includes two power MOSFET IRFP460 (500V-20A) and a PWM driver circuit (10 kHz, 60% duty-cycle). The DC input filter is composed of an electrolytic capacitor (3300 μF, 350 V) in parallel with a ceramic capacitor (0.33 μF, 400 V). The parasitic parameters of these elements were measured by means of a HP 4192A Impedance Analyzer. Their values are reported in Tab.I of the Appendix.

The chopper was supplied by a DC source (battery) of 100V and an ohmic load of 20 Ω was connected to the output.

For the EMI measurements, a HP 8590 Spectrum Analyzer was connected to the LISN signal terminals through a 24 dB attenuator. The analyzer was employed in the frequency range of 0.1-40 MHz (4 MHz/div) and with a vertical scale from 4 to 124 dBμV (15 dBμV/div). The bandwidth of the instrument was 3 kHz.

Fig.12 shows the peak spectrum envelope of the conducted emission measured with the heatsink of the power switches non-connected to ground. The corresponding numerical results are represented in Fig.5. A good agreement was achieved between the numerical and experimental results. In fact, Fig.12 clearly shows two peaks at the frequency of 700 kHz with an amplitude of 93 dBμV, and at the frequency of 32.1 MHz with an amplitude 68 dBμV (in the simulations we obtained 710 kHz, 95 dBμV and 31.8 MHz, 64 dBμV, respectively).

Fig.13 illustrates the peak spectrum envelope of the conducted emission measured with the heatsink connected to ground. The corresponding numerical results are represented in Fig.6. In this case, two further peaks are introduced. The additional peak at higher frequency occurs at 12.1 MHz with an amplitude of 75 dBμV. It is very close to the common-mode resonant peak obtained in the simulations (12.7 MHz, 80 dBμV). The additional peak at lower frequency is at about 4 MHz but it is not pointed out by the simulations.

Both Figs. 12 and 13 show a narrow peak at the frequency of about 10 MHz. Since the measurement environment was not screened, this peak could be imputed to SW radio interferences. In fact, it was present also when both the DC source and the MOSFET drivers were turned off.

5. Conclusions

In this paper, an analysis has been developed in order to emphasize how both differential- and common-mode components of the total conducted emission are generated in a switching cell that is the basic structure of most power converters. For this purpose, a detailed equivalent circuit has been proposed. This model permits the influence of the different parasitic components to be predicted. In particular, it has been shown that the peaks of the conducted emission spectrum are due to series LC resonant loops. The identification of these loops allows the frequency of the spectrum peaks to be predicted accurately. Furthermore, qualitative considerations on the amplitude of these peaks can be made.

The experimental tests on a DC chopper prototype substantially confirm both the theoretical analysis and the numerical results. We can summarize the main results as follows

a. The spectrum of the differential-mode EMI component presents two resonant peaks.

b. The capacitance of the electrolytic capacitor has in practice no influence on the resonant peaks.

c. The parasitic inductance of the electrolytic capacitor branch strongly affects the differential-mode resonant peak at lower frequency.

d. The capacitance of the ceramic capacitor affects only the differential-mode resonant peak at lower frequency.

e. The parasitic inductance of the ceramic capacitor affects the amplitude of the differential-mode interferences in a wide range of frequency.

f. The off-state capacitance of the power switches affects the differential-mode resonant peak at higher frequency.

g. The stray inductance of the switches branch affects the differential-mode resonant peak at higher frequency.

h. The presence of stray inductances between the LISNs and the chopper reduces the differential-mode interferences.

i. The ground connection of the heatsink introduces a path for common-mode currents through the capacitive coupling with the power switches. A common-mode resonant loop is created.

j. The parasitic capacitances between the power switches and the ground affect the common-mode resonant peak.

k. The stray inductance of the connecting wire between the heatsink and the ground affects the common-mode resonant peak.

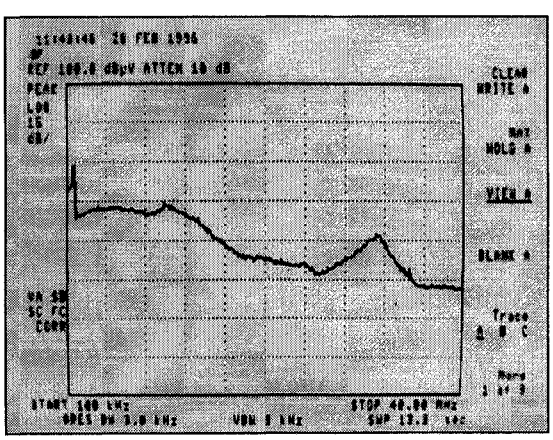

Fig.12: Measured peak spectrum envelope for the DC chopper: heatsink non-connected to ground

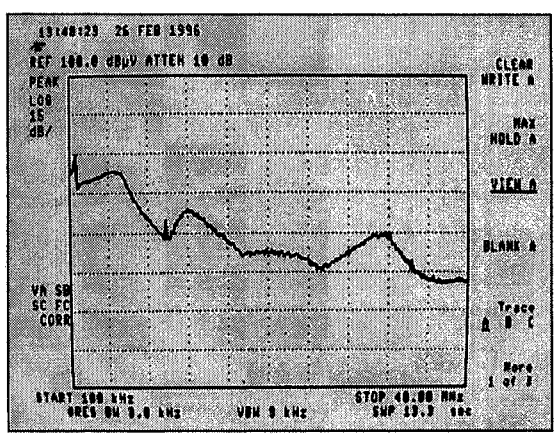

Fig.13: Measured peak spectrum envelope for the DC chopper: heatsink connected to ground

References

[1] P.A.Chatterton, M.A.Houlden, *EMC Electromagnetic theory to practical design.* WILEY 1992, Chichester, West Sussex (GB)

[2] L.Tihanyi, *Electromagnetic compatibility in power electronics.* IEEE Press 1995, New York (USA)

[3] M.Lardellier, G.Rojat, E.Labouré, F.Costa, *"EM disturbance in commutation cells for different technologies of silicon components."* EMC'94, 13-16 Sept. 1994, Roma (I), pp. 465-470

[4] R.Sheich, J.Roudet, *"EMI conducted emission in the differential mode emanating from an SCR: phenomena and noise level prediction."* IEEE Trans. PE, Vol. 10, N. 2, March 1995, pp. 105-110

[5] E.Labouré, F.Costa, C.Gautier, W.Melhem, *"Accurate simulation of conducted interferences in isolated DC to DC converters regarding to EMI standards."* PESC, Baveno (IT) June 23-27, 1996, pp. 1973-1978

[6] F.Bertha, B.Velaerts, E.Tatakis, *"An improved power diode model for Pspice, applied to converter simulation."* EPE'93, 13-66 Sept. 1993, Brighton (UK), pp. 249-254

[7] J.Pilacinski, *"A method for determining the parameters of power MOSFET and IGBT transistor models applied in the PSpice program."* EPE'95, 18-21 Sept. 1995, Sevilla (E), pp. 3.356-3.361

[8] E.Labouré, F.Costa, M.Lardellier, G.Rojat, *"Losses/EMI compromise relating to electrical constraints and components technology in static converters."* EPE'95, 18-21 Sept. 1995, Sevilla (E), pp. 3.340-3.345

[9] Klotz, J. Petzoldt, H.Volker, *"Experimental and simulative investigations of conducted EMI performance of IGBT for 5-10 kVA converters."* Proc. of the 27th Annual IEEE PESC, Baveno (Italy) June 23-27, 1996, pp. 1986-1991

Appendix

Table I: Main and stray parameters of the chopper

CONNECTING WIRES	CAPACITORS	MOSFETs
$R_{W1} = 0.1\ \Omega$	$C_{EL} = 3.3$ mF	$L_{D1} = 5$ nH
$L_{W1} = 0.2\ \mu H$	$L_{EL} = 34$ nH	$L_{S1} = 5$ nH
	$R_{EL} = 0.03\ \Omega$	$R_{G1} = 10\ \Omega$
$R_{W2} = 0.1\ \Omega$	$R_S = 10\ k\Omega$	$v_{G1} = 0 - 15$ V
$L_{W2} = 0.2\ \mu H$		
	$C_{CE} = 0.33\ \mu F$	$L_{D2} = 5$ nH
$R_{Wg} = 0.1\ \Omega$	$L_{CE} = 12$ nH	$L_{S2} = 5$ nH
$L_{Wg} = 1.1\ \mu H$	$R_{CE} = 0.05\ \Omega$	$R_{G2} = 10\ \Omega$
		$v_{G2} = 0 - 15$ V
$R_E = 0.5\ \Omega$	$C_{g1} = 50$ pF	
$L_E = 10\ \mu H$	$C_{g2} = 50$ pF	
$L_{WC} = 100$ nH		
$L_{SD} = 0$ nH		

Table II: Parameters of the LISN

RESISTORS	CAPACITORS	INDUCTORS
$R_m = 50\ \Omega$	$C_m = 0.33\ \mu F$	$L_1 = 250\ \mu H$
$R_b = 5\ \Omega$	$C_a = 0.47\ \mu F$	$L_2 = 50\ \mu H$
$R_a = 100\ \Omega$	$C_b = 8\ \mu F$	